Cancer Research

FLT3 and JAK2 Mutations in Acute Myeloid Leukemia Promote Interchromosomal Homologous Recombination and the Potential for Copy Neutral Loss of Heterozygosity

Terry J. Gaymes, Azim Mohamedali, Anthony L. Eiliazadeh, David Darling, and Ghulam J. Mufti

Abstract

Acquired copy neutral LOH (CN-LOH) is a frequent occurrence in myeloid malignancies and is often associated with resistance to standard therapeutic modalities and poor survival. Here, we show that constitutive signaling driven by mutated FLT3 and JAK2 confers interchromosomal homologous recombination (iHR), a precedent for CN-LOH. Using a targeted recombination assay, we determined significant iHR activity in internal tandem duplication FLT3 (FLT3-ITD) and JAK2V617F-mutated cells. Sister chromatid exchanges, a surrogate measure of iHR, was significantly elevated in primary FLT3-ITD normal karyotype acute myeloid leukemia (NK-AML) compared with wild-type FLT3 NK-AML. HR was harmonized to S phase of the cell cycle to repair broken chromatids and prevent iHR. Increased HR activity in G_0 arrested primary FLT3-ITD NK-AML in contrast to wild-type FLT3 NK-AML. Cells expressing mutated FLT3-ITD demonstrated a relative increase in mutation frequency as detected by thymidine kinase (TK) gene mutation assay. Moreover, resistance was associated with CN-LOH at the TK locus. Treatment of FLT3-ITD– and JAK2V617F-mutant cells with the antioxidant *N*-acetylcysteine diminished reactive oxygen species (ROS), restoring iHR and HR levels. Our findings show that mutated FLT3-ITD and JAK2 augment ROS production and HR, shifting the cellular milieu toward illegitimate recombination events such as iHR and CN-LOH. Therapeutic reduction of ROS may thus prevent leukemic progression and relapse in myeloid malignancies. *Cancer Res; 77(7); 1697–708. ©2017 AACR.*

Introduction

The majority of patients with adult acute myeloid leukemia (AML) that present with a normal karyotype (NK-AML) are grouped together in the "intermediate" risk cytogenetic category and constitute 40% to 45% of all adult AML patients. Mutations in the FMS-like tyrosine kinase 3 (FLT3) receptor whether it is internal tandem duplication (ITD) of its juxtamembrane domain or point mutations in its kinase domain are the most frequent mutations in NK-AML (1). Constitutive activation of the JAK2 signaling pathway occurs in most myeloproliferative neoplasms (MPN), such as Polycythaemia Vera, as well as in a significant proportion of other myeloid malignancies (2).Both FLT3-ITD and JAK2 mutations drive uncontrolled hematopoietic cell expansion. FLT3-ITD mutation in NK-AML predicts a more aggressive disease associated with resistance to therapy and poor survival. However, the prognosis for AML patients who have lost the WT FLT3 allele and acquired the mutated FLT3-ITD is worse compared with patients maintaining WT FLT3. LOH through duplication of genomic material on maternal or paternal chromosomes known as copy neutral LOH (CN-LOH) is a chromosomal change initially described in AML by Raghavan and colleagues (3). Since the discovery of CN-LOH (sometimes referred to as acquired uniparental disomy) in AML, recurrent regions of CN-LOH associated with homozygous mutations have been identified in AML (4). In addition to the CN-LOH of FLT3-ITD at 13q, CN-LOH has been demonstrated at 4q and 9p in the presence of homozygous mutations of TET2 and JAK2, respectively, doubling the oncogenic gene burden (5). Identification of multiple regions of LOH associated with mutation points to a common mechanism of homozygosity in myeloid malignancies that is required for leukemic progression.

It is now generally accepted that acquired CN-LOH is the result of a homologous recombination (HR) event (6). Mitotic HR is evoked in response to the repair of a double-strand break (DSB) in DNA. Genomic integrity is maintained in the cell by specific DNA repair mechanisms such as HR and nonhomologous end joining (NHEJ). Nonetheless, defects in DNA repair can result in the inappropriate or abnormal repair of DNA damage, resulting in propensity to malignant change. We have reported previously that primary AML cells have increased NHEJ repair activity and accompanying repair infidelity. Furthermore, constitutively activated N-RAS results in an increase in reactive oxygen species (ROS) that damages DNA and evokes a DNA damage response (7–9). Our

Department of Haematological Medicine, King's College London, Leukaemia Sciences Laboratories, The Rayne Institute, London, United Kingdom.

Note: Supplementary data for this article are available at Cancer Research Online (http://cancerres.aacrjournals.org/).

Corresponding Author: G. Mufti, King's College, Denmark Hill Campus, The Rayne Institute, 123 Coldharbour Lane, London SE5 9NU, United Kingdom. Phone: 44-207-346-3080; Fax: 44-207-733-3877; E-mail: ghulam.mufti@kcl.ac.uk

doi: 10.1158/0008-5472.CAN-16-1678

findings suggest that excessive DNA damage in AML may force normal DSB DNA repair components to process DSB aberrantly, resulting in chromosomal instability. It has been previously reported that constitutive FLT3 activation results in increased ROS production, a subsequent increase in DSB, and inaccurate repair by the NHEJ pathway (10). The authors suggested that genomic instability derived from constitutive FLT3 signaling generates more mutations that facilitate leukemic progression. However, increased NHEJ cannot account for phenomena of CN-LOH.

To explore the relationship between constitutive FLT3 and JAK2 signaling and the propagation of CN-LOH, we have utilized novel recombination assays that detect HR events in mutated FLT3 and JAK2 cells. We show that the FLT3-ITD and JAK2V617F mutations confer increased inter-HR (IHR, between chromosomes) activity compared with WT kinase. Moreover, iHR activity was reliant on the FLT3-ITD and JAK2V617F mutation–dependent elevation of ROS. NK-AML patients with FLT3-ITD mutations also possessed significantly increased sister chromatid exchanges (SCE, a surrogate for iHR activity), whereas a thymidine kinase (TK) reporter assay demonstrated that FLT3-ITD activity preferentially increases resistance to TK through the creation of CN-LOH. Our results pinpoint a common pathway whereby constitutive FLT3 and JAK2 signaling confers iHR and the subsequent propagation of CN-LOH in normal karyotype myeloid malignancy.

Materials and Methods

Patients

Twenty-two patients with *de novo* AML and normal karyotype by metaphase cytogenetics were selected. The median age was 53 years (8–78 years), and the median white blood cell count was 51.3×10^9/L. Primary material was obtained following written informed consent from patients prior to inclusion in study in accordance with the declaration of Helsinki by King's College Hospital Local Research Ethics Committee.

Drugs

The FLT3 inhibitor, AC220 (Quizartinib), was purchased from Selleckchem and resuspended in PBS. *N*-acetyl cysteine (NAC), hydrogen peroxide (H_2O_2), and the RAD51 inhibitor, B02, were purchased from Sigma-Aldrich.

Plasmids and DNA repair substrates

Human FLT3 and FLT3-ITD (18 bp insertion) have been previously cloned into FUGW plasmid (kind gift from Feyruz Rassool, University of Maryland, Baltimore, MD). The *BAMH*1-*ECOR*1 GFP fragment was removed from FUGW prior to cloning. Expression constructs, pMSCV-FLT3-WT and pMSCV-FLT3-ITD, were described previously (11–12) and were kindly donated by Lars Rönnstrand, University of Malmo, Sweden. PMSCVneo WT JAK2 and pMSCVneo JAKV617F (13) were kindly donated by Gary Reuther, University of South Florida, Tampa, FL. DNA repair substrate, DR-GFP, and the *I-SCE*I–expressing plasmid, pCBAS-CEI, have been described previously by Maria Jasin's group (14, 15) and were purchased via the Addgene repository (DR-GFP, Addgene plasmid 26475 and pCBASCEI, Addgene plasmid 26477). Creation of targeted repair substrates is provided in Supplementary Methodology.

Targeted recombination assays

To study targeted iHR, DNA repair substrates PZD-DR1-Puro (10 μg) and PZD-DR2-Blast (10 μg), were simultaneously transfected (Nucleofection; Amaxa) into 2×10^6 cells using the CompoZr Zinc finger nuclease (ZFN)–targeted integration Kit (Sigma) according to the manufacturer's instructions. To analyze targeted HR, PZD-DR1/DR2-Puro (20 μg) was transfected into 2×10^6 cells also using CompoZr ZFN. Two days after transfection, cells were antibiotic selected and divided into 24-well plates to isolate correctly targeted clones. After 5 days, cells were collected for FISH analysis and PCR identification of integration at the adeno-associated virus integration site (AAVS) locus. Only correctly targeted clones with PZD-DR1-Puro and PZD-DR2-Blast were selected and expanded. To correctly targeted HEK293 clones, 2 μg of WT, FLT3-ITD, JAK2V617F, or empty expression vector were transfected into 2×10^6 cells. Antibiotic selection (200 μg/mL Zeocin for FUGW-FLT3-ITD, 500 μg/mL G418 for pMSCVneo-JAK2V617F) was added 24 hours after transfection in fresh media. Relative expression of FLT3 and JAK2 was determined by qPCR and Western blotting 3 days after antibiotic selection. Ten microliter of the *I-SCE*I expression viral supernatant was added to PZD-DR1-Puro– and PZD-DR2-Blast–targeted cells and cultured for a further 5 days before FACS analysis. For simultaneous drug additions, 10 to 50 nmol/L AC220 or 5 mmol/L NAC were added for 24 hours prior to addition of *I-SCE*I. To account for variation in transfection efficiencies between test cells, the targeted recombination % for each test was made relative to the transfection of PZD-GFP-Puro GFP expression.

Cell lines

The leukemic cell lines, MOLM-13 and U937, the erythroleukemia cell line, HEL, and the embryonic kidney cell line, HEK293, were obtained from the DSMZ. The lymphoblastic cell line, TK6, was obtained from the ATCC. These cell lines were purchased within the last 3 years, propagated, expanded, and frozen immediately into numerous aliquots after arrival. The cells revived from the frozen stock were used within 10 to 15 passages and not exceeding a period of 6 months. The DSMZ and ATCC use morphological, cytogenetic, and DNA profile analysis such as short tandem repeat fragment analysis for characterization and authentication of cell lines. Prior to the study start, all cell lines were subjected to mutation analysis using Roche 454 parallel sequencing for authenticity compared with the genotype characterized by the DSMZ and ATCC.

PCR confirmations

To confirm specificity of targeted integration 5 days after transfection, DNA was prepared from transfected cells (Qiagen). Site-specific PCR was carried using the CompZr AAVS forward primer and a reverse primer specific to PZD-DR1-Puro and PZD-DR1/DR2-puro (5′-CTT GTA CAG CTC GTC CAT GC), and to PZD-GFP-puro and PZD-DR2-Blast (5′-CAG TGC AGG AAA AGT GGC ACT). PCR was carried out according to the CompZr integration PCR protocol using Roche Expand High Fidelity PLUS polymerase. To confirm the recombination at the I-*SCE*I site, recombined GFP-positive cells were FACS sorted (FACSaria; Beckman Coulter) into 96-well plates to collect GFP-positive cells. Cells were used for hot start PCR across the DR1 region using forward primer CTG CTA ACC ATG TTC ATG CC and reverse primer AAG TCG TGC TGC TTC ATG TG. The PCR product was digested with 10U of *I-SCEI* or 10U *BCG*1. GFP-positive PCR products attributable to HR should be *I-SCE*I un-digestible and *BCG*1 digestible. Products were loaded onto gels and stained with ethidium bromide, and the ethidium signals for the

enzyme-resistant and enzyme-cleaved band were quantified by using Adobe Photoshop software.

Fluorescent hybridization

PZD-targeting vectors were fluorescently tagged for FISH studies using the Fasttag labeling Kit (Vector). Ten microgram of vector was denatured at 95°C for 30 minutes in the presence of Fasttag reagent. Vectors were subsequently coupled with either fluorescein or Texas Red maleimide. Labeled vector DNA was determined to be between 100 and 400 bp by agarose gel electrophoresis. Metaphase spread chromosomes were prepared as stated for the analysis of SCE. After the slides were dried overnight, the slides were spotted with 200 μL ethanol and placed on a hotplate for 20 minutes. The slides were then cooled and immersed in 2% saline sodium citrate (SSC) for 20 minutes before dehydration in an ethanol series (70%, 85%, and 100%). Fluorescently labeled vector was diluted to 1 ng/μL in hybridization buffer (60% deionized formamide, 2 X SSC, 10% dextran sulfate, and 50 mmol/L sodium phosphate, pH 7). The fluorescently labeled vector was denatured at 75°C for 5 minutes prior to addition to the slide and sealing with rubber cement. The slide was then denatured on a hotplate for 4 minutes at 75°C. Slides were then placed in humid boxes overnight at 37°C. After hybridization, slides were blocked in blocking solution (5% non-fat dry milk plus 0.1% tween 20 in 4 X SSC) for 60 minutes at 37°C. The slides were then washed in blocking solution and subsequently incubated in biotinylated antifluorescein or anti–Texas Red (10 μg/mL) in blocking solution for 30 minutes at room temperature. Slides were washed again 3 times in blocking solution and then incubated in fluorescein or Texas Red Avidin solution (10 μg/mL) for 30 minutes at room temperature. Slides were washed in 4 x SSC + 0.1% tween 20 (2 × 5 minutes) before staining with DAPI (100 μg/mL) for 5 minutes and mounting in vectashield. SureFish 19q 13.11 CEBPA probe (Agilent) was used as a control for vector targeting the AAVS1 locus. Hybridization of probe was as per the manufacturer's instructions. Slides were visualized using a Leica epi-fluorescent microscope, and images were captured using a CCD camera and Leica LAS AF software. Two slides were prepared for each experiment.

TK6 assay

The lymphoblastoid cell line, TK6, was cultured in CHAT media (10 μmol/L deoxycytidine, 200 μmol/L hypoxanthine, 0.1 μmol/L aminopterin, and 17.5 μmol/L of thymidine) for 3 days to reduce the background mutant fraction. TK6 were then transfected with empty vectors, FUGW and pMSCV or FUGW WT-FLT3 and FUGW FLT3-ITD, selected in 200 μg/mL Zeocin or pMSCV-WT-FLT3 and pMSCV-FLT3-ITD selected in 1 μg/mL puromycin for 24 hours and then cultured for 5 days. To determine the mutation rate, 2×10^5 cells was seeded into ClonaCell-TCS Medium (Stem Cell Technologies) with and without 2 μg/mL trifluorothymidine (TFT) and incubated for a further 10 days. The mutation frequency was calculated by dividing the number of colonies on TFT-containing plates by the number of colonies on the plates without TFT. Triplicate plates for all tests were produced. The mutation rate was determined by seeding 2×10^5 cells into 25 wells of media containing TFT and determining the fraction of wells without TFT resistance. The mutation rate was calculated using the Fluctuation test originally described by Luria and Delbrück (16) using the following formula:

(ln - natural log, h – Number of wells without resistance/Total number of wells, n – Total number of cells).

Additional methods can be found in Supplementary Methodology.

Results

Development of a ZFN targeted assay for the determination of iHR

We firstly developed a novel reporter assay targeted to chromosome 19q using CompoZr Zinc finger nuclease (ZFN) to detect iHR (Fig. 1A–D). The assay, based on the DR-GFP reporter developed by Jasin and colleagues relies on the sequential targeting of two overlapping, but disrupted GFP repeat sequences to separate alleles at the AAVS1 locus (14–15). The two GFP repeat sequences, 5′GFP and 3′GFP, were individually cloned into the targeting vectors, PZDonor-AAVS1 Puromycin (Fig. 1A and C) and PZDonor (Fig. 1B and D), respectively, to create PZD-DR1-Puro and PZD-DR2-Blast, respectively. PZD-DR1-Puro and PZD-DR2-Blast can be sequentially targeted to AAVS1 on separate 19q alleles with concomitant transfection with AAVS1-specific ZFN. iHR and subsequent gene conversion between the disrupted GFP sequences would result in GFP expression. To test the specificity of ZFN targeting, we initially cloned the full-length intact GFP into PZDonor-AAVS puromycin and transfected this vector with AAVS1-specific ZFN into HEK293 cells. Supplementary Fig. S1A and S1B show correct integration of PZD-GFP-Puro into the AAVS1 locus using locus-specific primers and FISH. Integration efficiency before antibiotic selection was between 10% and 15% for cell lines (data not shown). Without ZFN transfection, there was no AAVS1 integration and no puromycin-resistant cells after selection. Targeted integration of PZD-DR1-Puro and PZD-DR2-Blast to the AAVS1 locus was performed in the FLT3-ITD–mutated cell line, MOLM-13 (known hereon as MOLM-13PZD), the WT FLT3 U937 (known hereon as U937PZD), and HEK293 (known hereon as HEK293PZD). Targeted integration was confirmed using locus-specific PCR and FISH (Fig. 1E–G). Clones with both the correct integration of PZD-DR1-Puro and PZD-DR2-Blast to separate AAVS1 loci were then expanded in culture.

FLT3-ITD cells demonstrate iHR

FLT3-ITD–expressing cells were tested for iHR events using the targeted iHR reporter assay. MOLM-13PZD– and FLT3-ITD–transfected HEK293PZD cells demonstrated reproducible GFP-positive cells in three separate experiments [iHR events, 0.15% and 0.25% respectively compared with U937PZD-, WT-FLT3–, and empty vector–transfected HEK293PZD cells (0%, $P < 0.05$, $n = 3$; Fig. 1H; Table 1)]. Induction of iHR in FLT3-ITD–transfected HEK293PZD corresponded to a 4-fold increase in RAD51 expression after normalization for FLT3 overexpression (Supplementary Fig. S2A). Pretreatment of MOLM-13PZD– and FLT3-ITD–transfected HEK293PZD cells with the FLT3 inhibitor, AC220, downregulated RAD51 expression with the concomitant abolition of iHR events (Fig. 1H; Supplementary Fig. S2B and S2C; Table 1). Furthermore, iHR were also eliminated with pretreatment with the antioxidant, NAC (Table 1; Supplementary Fig. S2B). Interestingly, iHR events were significantly dependent on both HR activity and ROS as pretreatment of MOLM-13PZD– and FLT3-ITD–transfected HEK293PZD cells with the RAD51 inhibitor, B02, abolished iHR events, but addition of the pro-oxidant,

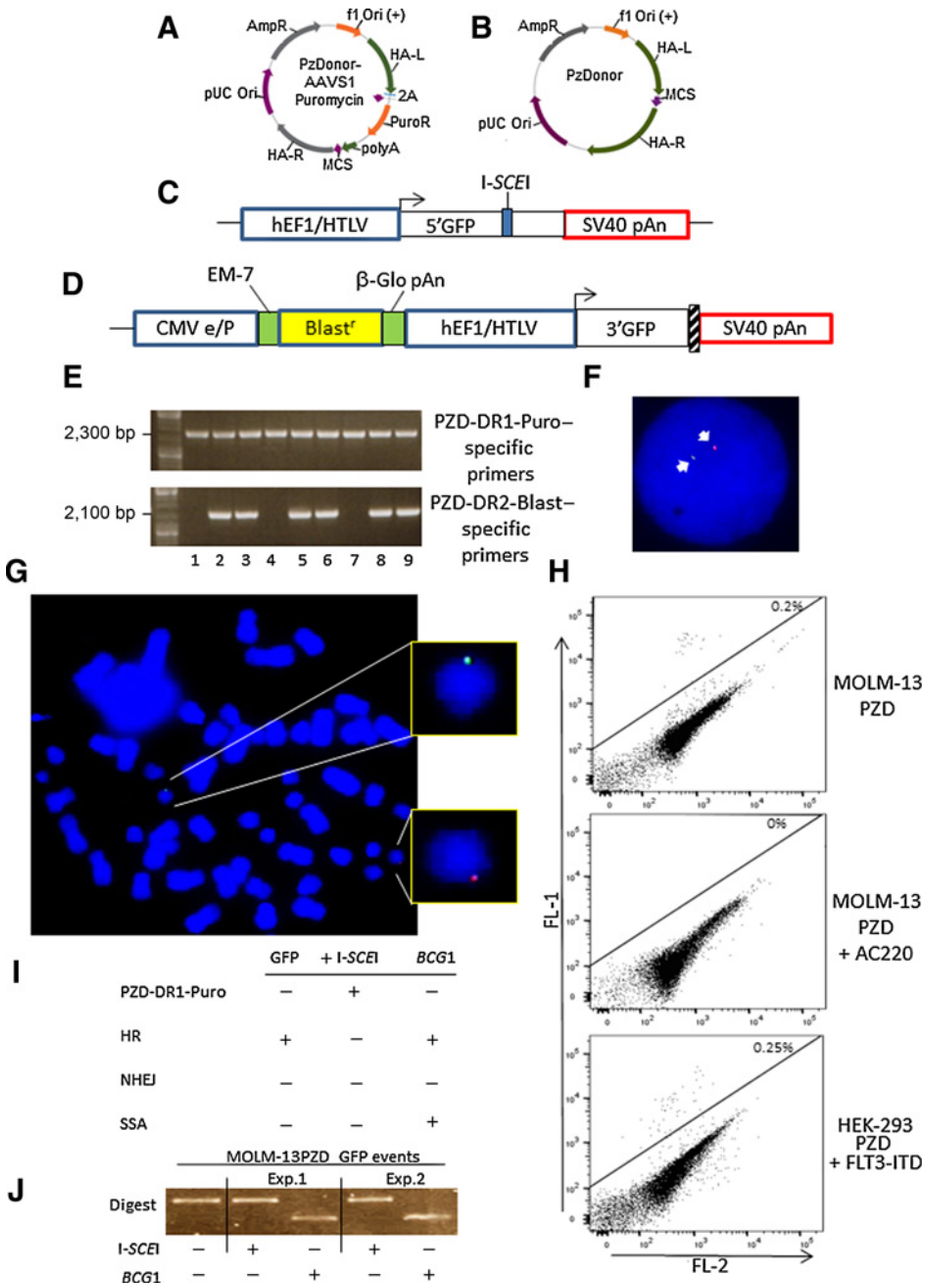

Figure 1.

ZFN-targeted assay for iHR demonstrates increased iHR in FLT3-ITD–mutated cells. **A** and **B,** Maps of targeting vectors, courtesy of Sigma-Aldrich. PZDonor-AAVS1 Puromycin (**A**) and PZDonor (**B**). HA, homology arm. **C,** DR1 insert possesses a 5′ GFP sequence interrupted by an 18 bp recognition sequence for *I-SCE*I. DR1 insert was cloned into the MCS of pZDonor-AAVS puromycin vector to create PZD-DR1-Puro. **D,** DR2-BLAST insert possesses a truncated 3′ GFP sequence. The construct was cloned into the MCS of pZDonor to create PZD-DR2-Blast. **E,** To confirm PZD-DR1-Puro and PZD-DR2-Blast integration at separate AAVS1 loci, vector- and ZFN-transfected cells were aliquoted into 24-well plates and individually checked for integration using PCR with vector- and locus-specific primers. Correct integration would produce a PCR product for PZD-DR1-Puro of 2300bp (top) and PZD-DR2-Blast of 2,100 bp (bottom). **F** and **G,** Co-FISH using a fluorescein-labeled PZD-DR1-Puro (green) and Texas Red–labeled PZD-DR2-Blast. Probes were sequentially hybridized to DAPI-stained cells (**F**) and metaphase chromosomes (**G**). Original magnification, ×100. **H,** FACS analysis of MOLM-13PZD, MOLM-13PZD pretreated with 25 nmol/L AC220, and FLT3-ITD–transfected HEK293PZD. To determine GFP recombination events, cells were analyzed using green (FL1) and orange (FL2) filters. Percentages of recombined GFP-positive cells (recombination events) were made relative to transfection of a targeted GFP-expressing plasmid. Top plot shows GFP+ve MOLM-13PZD cells, middle plot shows GFP+ve MOLM-13PZD cells with prior AC220 addition, and bottom plot shows FLT3-ITD–transfected HEK293PZD GFP+ve cells. **I** and **J,** Restriction digest of PZD-DR1-Puro PCR products indicates method of repair. Only GFP-positive cells would give *BCG*1-digestible PCR products. **J,** PCR products derived from GFP-recombined events from two separate experiments were digested with I-*SCE*I or *BCG*1. PCR products derived from MOLM-13PZD GFP recombination events were digestible with *BCG*1 and not I-*SCE*I.

Table 1. Summary of iHR-mediated events in mutant FLT3-ITD and JAK2V617F cells

	Targeted iHR (mean % ± SEM GFP cells)				
Cell	**Untreated**	**+ 25 nmol/L AC220**	**+ 5 mmol/L NAC**	**+ 25 μmol/L B02**	**+ 50 μmol/L H_2O_2**
MOLM-13PZD	0.15 ± 0.05	0	0	0	0.25 ± 0.05
U937PZD	0	0	0	0	0
HEK293PZD + EV	0	0	0	0	0
HEK293PZD + WT FLT3	0	0	0	0	0
HEK293PZD + FLT3-ITD	0.25 ± 0.05	0	0	0	0.4 ± 0.05
HELPZD	0.2 ± 0.05	0	0	0	0.15
HEK293PZD + WT JAK2	0	0	0	0	0
HEK293PZD + JAK2V617F	0.3 ± 0.05	0	0	0	0.4 ± 0.05

NOTE: Percentages are the result of replicate studies ($n = 3$).

H_2O_2 increased iHR events (Table 1; Supplementary Fig. S2B). To verify that GFP-positive cells in this assay were the result of iHR and not false positives, hot start PCR using primers designed at the DR1 locus was carried out on FACS-sorted GFP-positive cells. PCR products from GFP-positive cells could only be digested by *BCG*1 and not *I-SCE*I, confirming the presence of iHR-dependent GFP-positive cells (Fig. 1I and J). GFP-positive cells were also verified using fluorescence microscopy (Supplementary Fig. S2D).

FLT3-ITD mutation increases HR events in primary NK-AML. Increased HR has been shown previously in FLT3-ITD AML (17). To investigate further the presence of elevated HR as the catalyst for iHR in primary FLT3-mutated AML, we measured targeted single locus HR in a cohort of NK-AML. Primary NK-AML ($n = 22$) were initially characterized by SNP-A and DNA sequencing (Supplementary Table SI). Fifteen of 22 primary NK-AML had FLT3-ITD mutations with a clone size ≥25%. Seven of 22 primary NK-AML were WT for FLT3, but had nucleophosmin (NPM1) and DNA methyltransferase 3 (DNMT3a) mutations. We developed a novel HR reporter assay, using the HR substrate, PZD-DR1/DR2-Puro that possesses two disrupted, but overlapping, GFP sequences targeted to AAVS1 (Supplementary Fig. S3A; Supplementary Information). HR between the two sequences would result in GFP expression. PZD-DR1/DR2-Puro was transfected into primary FLT3-ITD with CompoZr ZFN. Supplementary Fig. S3B and S3D show correct integration of PZD-DR1/DR2-Puro into the AAVS1 locus using locus-specific primers and FISH. Clones with the correct integration of PZD-DR1/DR2-Puro AAVS1 were further transfected with an *I-SCE*I expression viral supernatant to introduce a DSB in the integrated PZD-DR1/DR2-Puro and induce recombination. PZD-DR1/DR2-Puro/*I-SCE*I–transfected primary FLT3-ITD ($n = 4$) demonstrated significantly increased HR activity compared with primary WT FLT3 ($n = 2$; 1.2% vs. 0.25%; $P < 0.01$; Fig. 2A; Supplementary Table SII). The increased HR activity was not attributable to elevated I-*SCE*I expression in primary FLT3-ITD after lentiviral transduction, but minimal cytotoxicity was noted at high I-*SCE*I concentrations in all primary cells that did not affect recombination rates (Supplementary Fig. S4A). All measurements of PZD-DR1/DR2-Puro HR events were made relative to transfection of PZD-GFP-Puro + ZFN to correct for variable transfection efficiencies in primary AML. Integration efficiency before antibiotic selection was between 5% and 15% for primary cells (Supplementary Fig. S4B). Pretreatment of primary cells with AC220 or NAC significantly inhibited HR events (1.2% vs. 0.1%; $P < 0.01$; Fig. 2A; Supplementary Table SII). Moreover, PZD-DR1/DR2-Puro/*I-SCE*I–transfected MOLM-13 and U937 + FLT3-ITD also exhibited increased targeted HR that was inhibited with AC220 or NAC (mean across all groups, 2.6% vs. 0.35%; $P < 0.01$; Supplementary Table SIII; Supplementary Fig. S4C–S3D). Inhibition of HR in primary NK-AML correlated with the reduction in RAD51 expression with AC220 (Fig. 2B). Expression of HR repair factors, MRE11 and CTiP, was not affected by AC220, but the expression of cyclin-dependent kinase inhibitor, p21, was abrogated as previously shown by Raderschall and colleagues (18). FLT3-ITD expression also resulted in the phosphorylation of both AKT and STAT5 in primary NK-AML– and FLT3-ITD–transfected HEK293 that was also abrogated upon AC220 pretreatment (Fig. 2B and C). Mononuclear cells from this cohort of primary NK-AML–, MOLM-13–, and FLT3-ITD–transfected U937 were also cultured and assessed for their ability to localize phospho-γH2AX and RAD51 as a measure of DSB DNA damage and HR activity, respectively. Immunofluorescence studies showed that primary AML with FLT3-ITD–, MOLM-13–, and FLT3-ITD–transfected U937 cells has increased mobilization of phospho-γH2AX and RAD51 compared with WT FLT3 primary AML cells and U937 transfected with WT FLT3 (mean for all groups; RAD51, 21% vs. 10.3%, $P < 0.01$; phospho-γH2AX, 17% vs. 12.7%, $P < 0.01$, $n = 3$; Fig. 2D and E; Supplementary Fig. S5A–S5C). Pretreatment of cells with NAC significantly inhibited both RAD51 foci formation (21% vs. 14%, $P < 0.01$) and phospho-γH2AX foci (17% vs. 11.6%, $P < 0.05$). Moreover, there was a direct correlation between the increased RAD51 and phospho-γH2AX foci and the augmentation of ROS for FLT3-ITD–positive NK-AML (Fig. 2E and F; Supplementary Fig. S5A–S5E).

Primary AML with FLT3-ITD mutations demonstrate increased SCE

Given the increased HR in mutated FLT3 cells, recombination or "crossing over" is likely to occur between chromatids following DNA breakage. This phenomenon is known as SCE. Inadvertent slippage of a broken chromatid could result in the use of its homologous chromosome for repair, supporting the utility of SCE analysis as a surrogate for iHR. To confirm the presence of elevated recombination in primary FLT3-mutated AML, we measured SCE in 22 NK-AML. FLT3-ITD primary AML–, MOLM-13–, and FLT3-ITD–transfected U937 cells show a significant increase in SCE compared with WT FLT3 primary AML– and WT FLT3–transfected U937 (mean across groups, 9.9 vs. 5.5 SCE per metaphase, $P < 0.001$; Fig. 2G and H; Supplementary Fig. S6A–S6C; Supplementary Tables SII and III). Moreover, treatment of FLT3-ITD primary AML–, MOLM-13–, and FLT3-ITD–transfected U937 cells with the AC220 or NAC restored SCE to levels observed for WT FLT3 (mean across groups AC220: 9.9 vs. 5.9 SCE per metaphase, $P < 0.05$; NAC: 9.9 vs. 6.7 SCE per metaphase, $P < 0.05$).

JAK2V617F mutation increases targeted iHR events

Constitutive activation of the JAK2 signaling pathway occurs in most MPN, such as Polycythaemia Vera, as well as in a significant

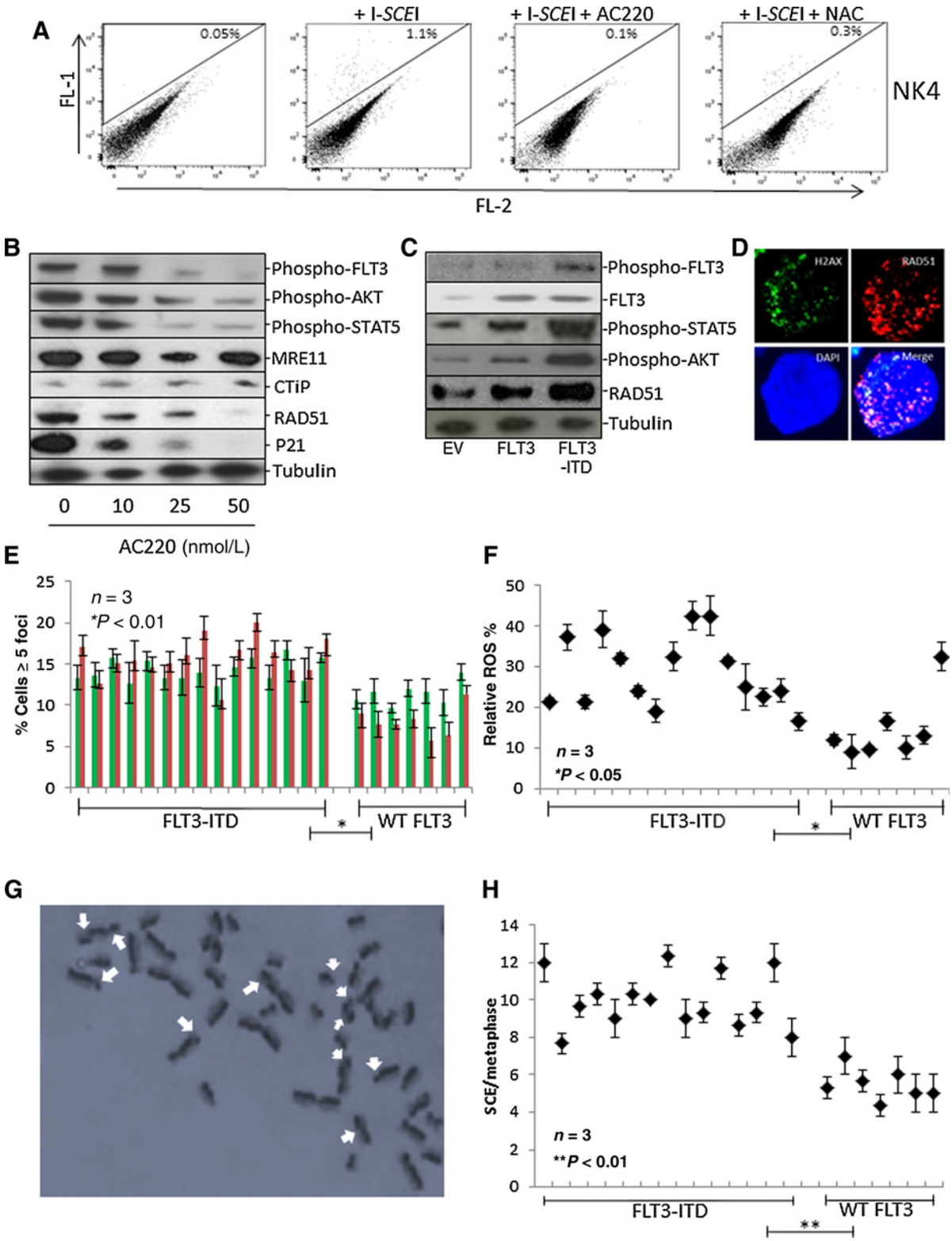

Figure 2.

Mutant FLT3-ITD increases HR activity and events in primary NK-AML. **A,** FACS analysis of PZD-DR1/DR2-Puro–targeted cells in primary FLT3-ITD NK-AML (NK4). GFP-positive cells (recombination events) were analyzed using green (FL1) and orange (FL2) filters. Recombination events were made relative to transfection of a targeted GFP-expressing plasmid. (*Continued on the following page.*)

proportion of other myeloid malignancies. JAK2 mutations such as V617F give rise to a proliferative phenotype that has also shown to induce increased ROS production (19). As JAK2V617F is associated with CN-LOH on chromosome 9p in MPN, we determined whether JAK2 and FLT3 mutations share a common mechanism in initiating CN-LOH. The JAK2V617F-mutated leukemic cell line, HEL, and JAK2V617F-transfected HEK293 demonstrated 4-fold increased RAD51 expression compared with U937 and WT JAK2–transfected HEK293 (Fig. 3A and B). JAK2V617F expression also resulted in the phosphorylation of both AKT and STAT5 in JAK2V617F-transfected HEK293. Targeted integration of PZD-DR1-Puro and PZD-DR2-Blast to the AAVS1 locus was performed in the JAK2V617F-mutated cell line, HEL (known hereon as HELPZD), and showed significant iHR events compared with U937PZD (0.2% vs. 0%, $P < 0.05$, $n = 3$; Fig. 3C). Furthermore, we were able to abolish iHR events with NAC. HEK293PZD cells were transfected with JAK2V617F and also demonstrated reproducible GFP-positive cells (iHR events, 0.3% compared with WT JAK2– and empty vector–transfected HEK293PZD cells; 0.3% vs. 0%, $P < 0.05$, $n = 3$; Table 1). We also show that HEL- and JAK2V617F-transfected HEK293 cells demonstrate increased HR compared with HEK293 + WT JAK2 (2.6% vs. 1%, $P < 0.05$, $n = 3$) and that ROS is significantly elevated in JAK2V617F cells (Fig. 3D–F).

Inappropriate RAD51 expression and HR activity in G_0-arrested FLT3-ITD cells

RAD51 expression is tightly regulated in normal cells with the highest expression being at S–G_2 phases during and after DNA replication and its lowest expression at G_0–G_1 phases or in nondividing cells (6). As FLT3-ITD mutation results in significantly overexpressed RAD51, we investigated whether there was inappropriate expression of RAD51 in FLT3-ITD–mutated cells outside of S–G_2 that may result in recombination between homologous chromosomes rather than between identical chromatids after replication. Primary NK-AML and MOLM-13 cells were initially cultured in full growth media and then in the absence of FCS for 3 days. G_0-arrested primary FLT3-ITD NK-AML and G_0-arrested and FACS-sorted MOLM-13 demonstrated increased RAD51 foci localization and low, but consistent, RAD51 expression compared with G_0-arrested primary WT FLT3 AML (Fig. 4A–D) and G_0-arrested FACS-sorted U937 cells (Supplementary Fig. S7A–S7F). Strikingly, G_0-arrested WT FLT3 primary AML and G_0-arrested U937 cells only exhibited RAD51 expression 12 hours after culture stimulation with growth factors. Transfection of the HR substrate, PZD-DR1/DR2-Puro, and subsequent induction of a DNA DSB by I-*SCE*I transfection showed that G_0-arrested FACS-sorted MOLM-13 demonstrated low, but reproducible, HR events compared with G_0-arrested FACS-sorted U937 cells. Furthermore, G_0 MOLM-13 HR events were abolished with coculture with AC220 or NAC (Fig. 4G).

FLT3-ITD mutation promotes CN-LOH over hemizygosity at the TK locus

The human lymphoblastic cell line, TK6, possesses heterozygous frameshift mutations in exons 4 and 7 of TK (20). LOH at this locus renders resistance to TFT. We exploited LOH at the TK locus to study the effects of mutant FLT3-ITD expression. TK6 cells were transfected with FLT3-ITD or WT FLT3 or empty vectors and subsequently cultured in TFT to allow the generation of TK mutations. Figure 5A and Supplementary Table SIV show that spontaneous TK mutation rate and frequency were significantly elevated in FLT3-ITD–transfected TK6 clones compared with WT FLT3– and empty vector–transfected TK6 clones. We demonstrated this mutation phenotype using two different FLT3-ITD–expressing vectors (FUGW and pMSCV). Strikingly, for both FLT3-ITD–expressing vectors, mutant rate and frequency were significantly ameliorated with addition of AC220 or NAC. To determine the type of LOH if any at the TK locus, clones from FLT3-ITD, WT FLT3, and empty vector controls were used for fragment PCR analysis. More than 20 TK-deficient clones were analyzed per group. Figure 5B and C demonstrates that in FLT3-ITD–transfected TK6 mutants, more than 50% of clones exhibited homozygous LOH at the TK locus in contrast to empty vector controls. The remaining 50% in FLT3-ITD–transfected TK6 gave no LOH, whereas hemizygous LOH was not observed. Significantly, CN-LOH frequency at the TK locus was inhibited with concomitant addition of AC220 (55% vs. 28%, $P < 0.01$) and NAC (55% vs. 26%, $P < 0.01$). Microsatellite analysis of the q arm of chromosome 17 was also used to confirm CN-LOH in TK mutants. Nine microsatellites were chosen, eight located to the q arm and one to the p arm. From 34 TK-resistant colonies derived from FLT3-ITD–transfected TK6 clones, we determined three sizes of CN-LOH all extending to the telomere (Fig. 5D). FLT3-ITD–transfected TK mutants demonstrating homozygous LOH at the TK locus establish an enhanced propensity of such mutations to confer CN-LOH and can be abrogated through inhibition of constitutive FLT3 activity or antioxidant treatment.

Discussion

Oncogenes such as FLT3 and JAK2 play key roles in hematopoietic stem cell proliferation, differentiation, and survival (21–23). Mice that are heterozygous for the FLT3-ITD mutation develop a chronic myeloproliferative disease and must acquire other mutations or cellular changes to develop the full AML phenotype. Other molecular changes must also occur to allow the spontaneous LOH in these oncogenes that increases the severity of AML. Since our original report detailing CN-LOH in low-risk myelodysplastic syndrome (24), there have been a plethora of reports documenting the prevalence of CN-LOH in a number of other hematologic disorders (reviewed by O'Keefe and colleagues; ref. 4). Furthermore, we and others have associated microsatellite

(*Continued.*) **B** and **C,** Expression of DNA damage and growth signaling proteins were analyzed by Western blotting. Immunoblots were prepared from whole-cell extracts of primary NK-AML (NK4) pretreated with AC220 for 4 hours prior to harvest (**B**) and whole-cell extracts of transfected U937 with WT-FLT3, FLT-ITD, or empty vector (**C**). Tubulin acted as a loading control. **D–F,** HR repair analyzed by immunohistochemistry for phospho-γH2AX and RAD51 foci. **D,** Composite figure of foci formation in FLT3-ITD–mutated primary NK-AML cells (NK-10). Original magnification, ×100. **E,** Frequency of cells displaying greater than 5 foci per cell in primary AML. **F,** Graph of relative ROS percentage in primary NK-AML. Error bars, mean ± SEM of three separate experiments. **G** and **H,** SCE analysis of primary NK-AML. **G,** Metaphase spreads of SCE from primary NK-AML cells (NK4). **H,** Graph of SCE. Error bars, mean ± SEM of three separate experiments. At least 50 cells in metaphase were counted per test. Error bars, mean ± SEM of three separate experiments. Original magnification, ×100.

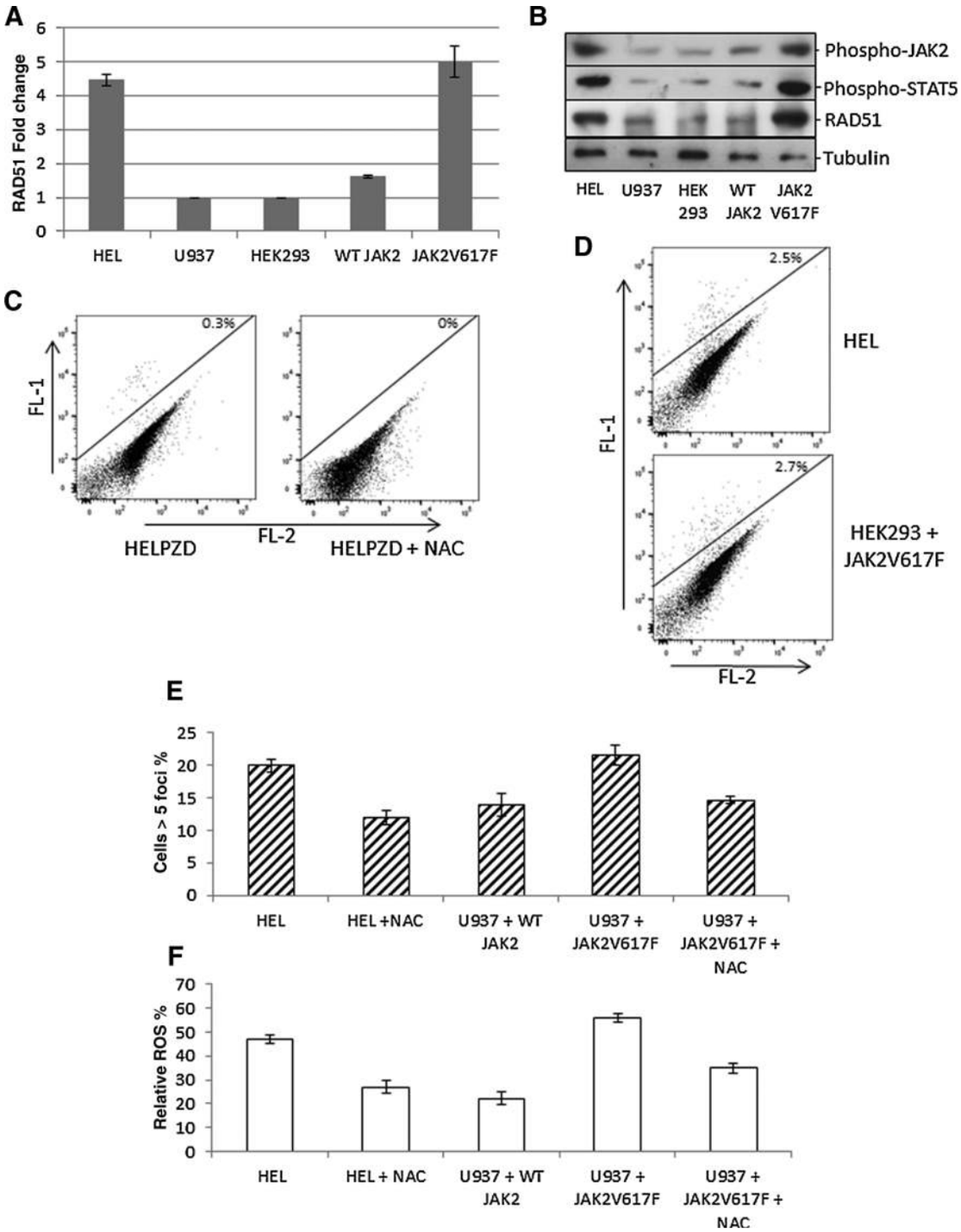

Figure 3.

Mutant JAK2V617F confers iHR associated with increased HR activity and ROS. **A** and **B,** RAD51 expression by qPCR and Western blotting in HEL (JAK2V617F), U937 (WT JAK2), HEK293 (WT JAK2) + empty vector (EV), HEK293 + WT JAK2, and HEK293 + JAK2V617F. **A,** cDNA relative target abundance (fold change) was normalized against the housekeeping genes GAPDH, tubulin, and B2M and then normalized to JAK2 expression. **B,** Immunoblots were prepared from whole-cell extracts of HEL cells and WT-JAK2, JAK2V617F, or empty vector–transfected HEK293. Tubulin acted as a loading control. **C** and **D,** iHR and HR activity in JAK2V617F-mutated cells. **C,** iHR events in JAK2V617F-mutated HEL cells (HELPZD). Cells were pretreated with NAC where indicated for 5 days prior to analysis. Left plot shows GFP+ve cells without NAC, right plots show GFP+ve cells with NAC pretreatment. **D,** HR events in PZD-DR1/DR2-Puro–targeted HEL cells (top) and JAK2V617F-transfected HEK293 (bottom). To determine DR-GFP recombination events, cells were analyzed using green (FL1) and orange (FL2) filters. Percentage of recombined GFP-positive cells (recombination events, inset %) was made relative to transfection of a targeted GFP-expressing plasmid. **E,** Frequency of cells displaying greater than 5 foci per cell for RAD51 foci in transfected cell lines. Two hundred nuclei were counted per experiment. Error bars, mean ± SEM of three separate experiments. **F,** Graph of relative ROS % in WT JAK2 or JAK2V617F cells. Error bars, mean ± SEM of three separate experiments.

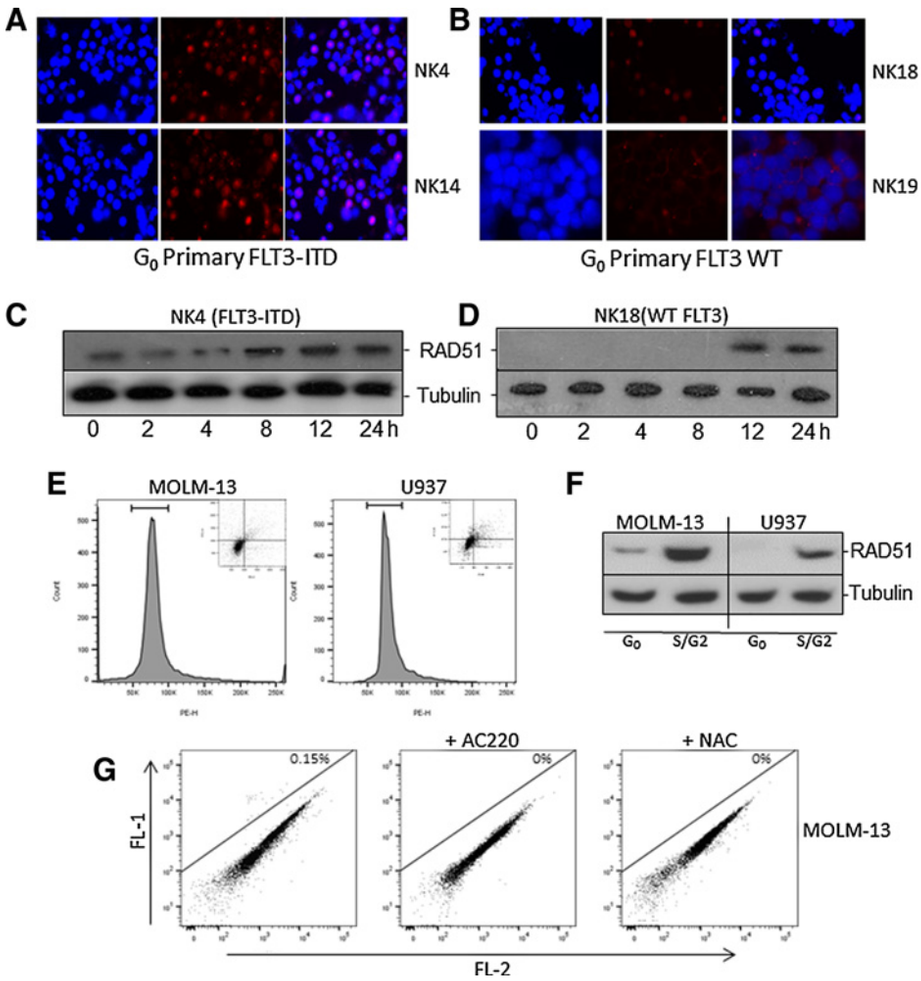

Figure 4.

G_0-arrested FLT3-ITD mutants demonstrate RAD51 expression and significant HR activity. **A** and **B,** Composite representation of RAD51 foci in G_0-arrested primary FLT3-ITD NK-AML (**A**) and G_0-arrested primary WT FLT3 NK-AML (**B**) by immunocytochemistry. Original magnification, ×40. **C** and **D,** Identification of RAD51 expression in G_0-arrested primary NK-FLT3-ITD AML (**C**) and G_0-arrested primary WT FLT3 NK-AML (**D**) by Western blotting. Immunoblots were prepared from whole-cell extracts of primary NK-AML and probed with anti-RAD51. Tubulin acted as a loading control. **E,** Cell-cycle kinetics of G_0-arrested MOLM-13 and U937. Arrested cells determined as G_0 phase (histogram peak and dot plot bottom left quadrant cells, inset) were collected by FACS sorting. **F,** G_0 and S–G_2 FACS-sorted cells were analyzed for RAD51 expression by Western blotting in MOLM-13 and U937. Tubulin acted as a loading control. **G,** FACS analysis of PZD-DR1/DR2-Puro–transfected G_0-arrested MOLM-13 with and without prior treatment with AC220 or NAC. To determine HR events, cells were analyzed using green (FL1) and orange (FL2) filters. Percentage of recombined GFP-positive cells (recombination events) was made relative to transfection of a targeted GFP-expressing plasmid.

instability as an instigator of CN-LOH (25–26). However, the etiology of CN-LOH acquisition remains unknown. In this report, we provide comprehensive evidence of a common mechanism of CN-LOH in NK-AML where excessive ROS-derived DSB DNA damage is preferentially repaired by mutant FLT3– or JAK2-dependent elevation in iHR and HR.

ROS has been previously shown to be elevated by mutant FLT3 (10), JAK2 (19), and BCR-ABL (27), resulting in DNA damage, genomic instability, and leukemic progression. Indeed, we have previously demonstrated that a constitutively activated mutant N-RAS mouse model augments ROS production, resulting in DSB DNA damage and subsequent upregulation of NHEJ repair activity. Mice fed with the antioxidant, NAC demonstrated a significant reduction in ROS, diminished DNA damage, and NHEJ activity (9). We demonstrate here that mutant FLT3 and JAK2 confer augmented ROS species that induce DNA damage, resulting in both mutations and chromosomal instability as observed in the TK assay that can be abolished with pretreatment with antioxidants. Such genomic instability is the prerequisite for leukemic progression. Interestingly, both STAT5 and AKT were phosphorylated in FLT3-ITD and JAK2V617F cells. STAT5-dependent activation of NADPH oxidase in association with RAC1 results in increased ROS, whereas AKT activates FOXO3 to abrogate catalase (inhibitor of ROS; ref. 28). A contribution of both pathways is likely to provide the high levels of ROS to drive genomic instability and leukemic progression.

Repair of DSB requires the co-ordinated actions of both NHEJ and HR to insure genomic fidelity and negate chromosomal aberrations. NHEJ is the predominant mammalian pathway being active throughout the cell cycle, whereas HR is primarily active during S phase during DNA replication. Aberrant interplay between these repair activities has a profound effect on DNA repair and genomic fidelity. In accordance with other reports, mutant FLT3 and JAK2 demonstrated increased RAD51 expression, resulting in exaggerated HR activity through the binding of phosphorylated STAT5 to the RAD51 promoter (29). It is notable that mutants FLT3 and JAK2 are associated with CN-LOH at their respective loci, resulting in a more aggressive phenotype. Similarly, mutant TP53 that is also associated with CN-LOH at 17p demonstrates increased RAD51 expression and HR activity (29). The elevated HR activity not only results in increased resistance to traditional chemotherapy, but could also drive the propagation of iHR. Here, we provide a model where FLT3-ITD– and JAK2V617F-dependent constitutive activity drives the propagation of CN-LOH that can be prevented with antioxidant treatment (Fig. 5E). Mutated FLT3 or JAK2 drives the accumulation of ROS that damages DNA and is preferentially repaired by FLT3-ITD– and JAK2V617F-dependent augmentation of the HR repair pathway

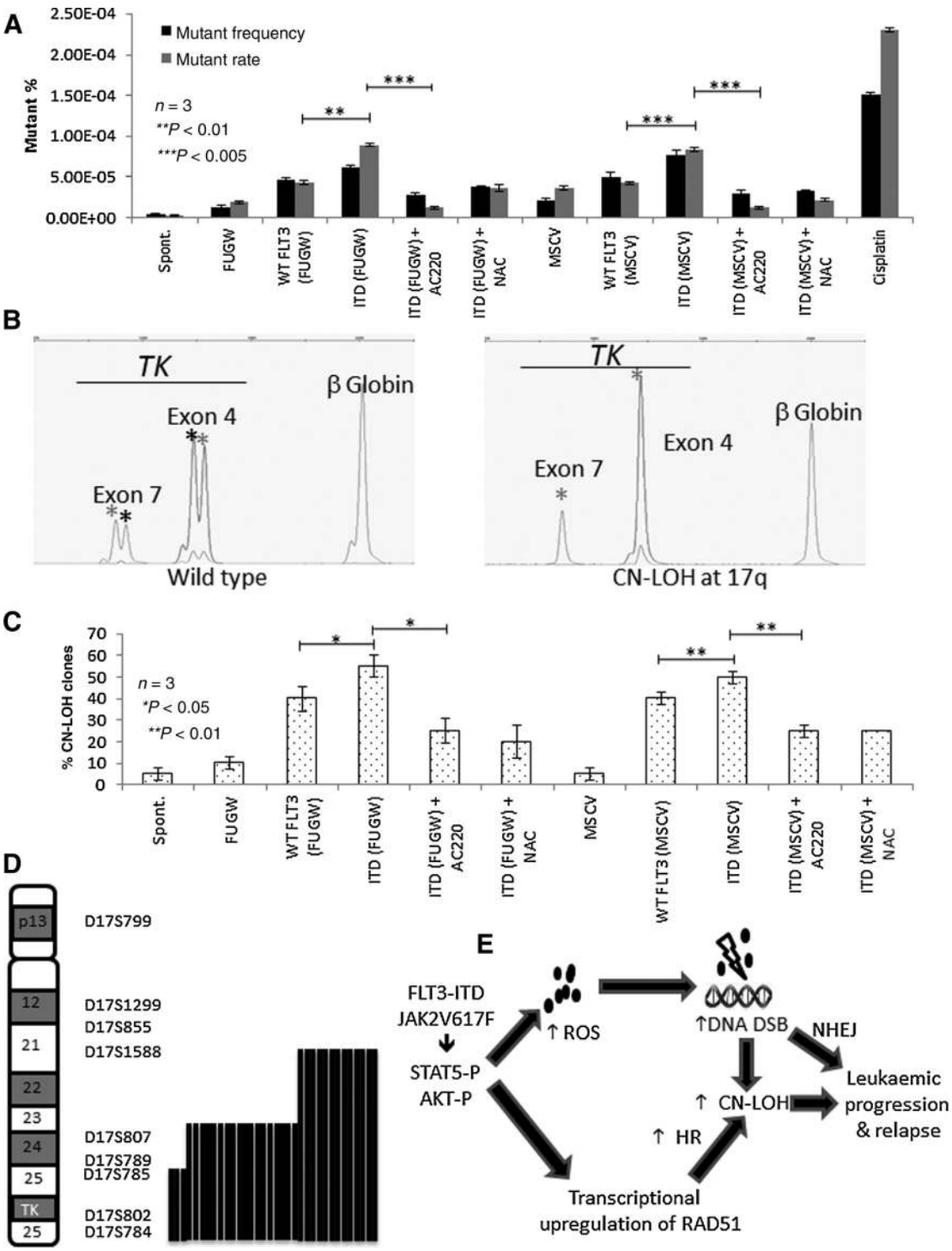

Figure 5.

Spontaneous TK mutation rate and frequencies of TK6 cells transfected with FLT3-ITD– and WT FLT3–expressing vectors or controls. **A,** Mutation rate and frequencies in transfected TK6 cells treated with and without AC220 or NAC. Error bars, mean ± SEM of three separate experiments. **B,** Mutation spectrum at the TK locus. Fragment fluorescent PCR was used to determine the presence of LOH. Mutants with double peaks (left) for each exon were considered WT at the TK locus. Mutants with single peaks have LOH. Comparison of peak areas relative to the peak area for β-globin can be used to distinguish CN-LOH and hemizygous LOH. CN-LOH (right) had double peak area compared with hemizygous LOH. **C,** Graph of CN-LOH TK mutants from transfected TK6 treated with and without AC220 or NAC. Error bars, mean ± SEM of three separate experiments. **D,** Determination of CN-LOH regions at the TK locus. Fluorescent fragment PCR of heterologous microsatellites at the TK locus was analyzed to determine the extent of LOH in FLT3-ITD TK-mutant clones. Approximate position of each microsatellite is stated. Human TK locus maps to 17q25. Length of bars indicates size of CN-LOH at the TK locus. **E,** Proposed model of the collaborative activities of ROS and HR to create CN-LOH in mutated FLT3 myeloid malignancy.

that increases SCE and also the likelihood of increased iHR events. A specific iHR event at 13q for FLT3 or 9p for JAK2 would result in the doubling of mutant gene dosage and selection for malignant progression. However, the observed overactive HR may not by itself be sufficient to confer iHR. To this end, we also demonstrate inappropriate expression of HR activity in G_0 cells in primary FLT3-ITD cells. HR is tightly regulated to be active after DNA replication to repair broken chromatids. Breaks in one chromatid can be accurately repaired using its identical sister by HR. Prior to DNA replication in G_1, NHEJ repairs DSB; however, illegitimate HR expression in G_1 has the capacity to repair breaks between homologous chromosomes, resulting in iHR events and CN-LOH. Further, we show that mutated FLT3 also confers increased expression of the cyclin-dependent kinase inhibitor, p21, in primary NK-AML, mediating G_1 arrest and slower progression to S phase increasing the likelihood for iHR.

The proposal that CN-LOH is not merely a stochastic event brought about by selection pressure of a leukemic clone, but a direct result of constitutional FLT3 and JAK2 activity has considerable relevance to the biology and therapy of myeloid malignancies. The disparate and independent activities of a single oncogene having the capacity to combine to create CN-LOH may be a common mechanism in these diseases. The identification of this mechanism of CN-LOH propagation will also open up further avenues of investigation. The TK assay revealed a bias in FLT3-ITD–transfected cells to specific sites and sizes of CN-LOH. The uniformity of the CN-LOH suggests that common breakpoints at the TK locus were responsible for the CN-LOH. Similarly, CN-LOH at 13q may be a reflection of hotspots of recombination at the locus rather than simply a selection of a mutant FLT3 homozygous clone. Targeting integration of DNA repair substrates at CN-LOH rich loci could be utilized to determine preferential sites of recombination and their correlation to fragile sites. ROS-induced DNA damage has been postulated to induce mutations to accelerate leukemic progression and relapse (9). The present study makes a valid case for the use of antioxidants in hematologic malignancy given the observed ROS accumulation in CML, AML, MPN, and CLL (30). Such treatments working alone or in combination with conventional therapies could prevent the accumulation of mutations and the acquisition of CN-LOH in NK-AML, slowing the rate of disease progression. Furthermore, the side effects of using high-dose DNA-damaging chemotherapy could be avoided if low doses can be combined with antioxidants. Our findings suggest that novel therapies targeting the generation of ROS would prove to be of great importance clinically for treatment of mutant FLT3 and JAK2 myeloid malignancies.

Disclosure of Potential Conflicts of Interest

No potential conflicts of interest were disclosed.

Authors' Contributions

Conception and design: T.J. Gaymes, G.J. Mufti
Development of methodology: T.J. Gaymes, G.J. Mufti
Acquisition of data (provided animals, acquired and managed patients, provided facilities, etc.): T.J. Gaymes, A. Mohamedali, A.L. Eiliazadeh, D. Darling
Analysis and interpretation of data (e.g., statistical analysis, biostatistics, computational analysis): T.J. Gaymes, A. Mohamedali, A.L. Eiliazadeh, G.J. Mufti
Writing, review, and/or revision of the manuscript: T.J. Gaymes, A. Mohamedali, G.J. Mufti
Administrative, technical, or material support (i.e., reporting or organizing data, constructing databases): T.J. Gaymes
Study supervision: T.J. Gaymes, G.J. Mufti

Grant Support

This study was supported by National Health Service UK.

The costs of publication of this article were defrayed in part by the payment of page charges. This article must therefore be hereby marked *advertisement* in accordance with 18 U.S.C. Section 1734 solely to indicate this fact.

Received June 23, 2016; revised December 9, 2016; accepted January 4, 2017; published OnlineFirst January 20, 2017.

References

1. Martelli MP, Sportoletti P, Tiacci E, Martelli MF, Falini B. Mutational landscape of AML with normal cytogenetics: Biological and clinical implications. Blood Rev 2013;27:13–22.
2. Valentino L, Pierre J. JAK/STAT signal transduction: Regulators and implication in hematological malignancies. Biochem Pharmacol 2006;71:713–21
3. Raghavan M, Smith LL, Lillington DM, Chaplin T, Kakkas I, Molloy G, et al. Segmental uniparental disomy is a commonly acquired genetic event in relapsed acute myeloid leukemia. Blood 2008;112:814–21
4. O'Keefe C, McDevitt MA, Maciejewski JP. Copy neutral loss of heterozygosity: A novel chromosomal lesion in myeloid malignancies. Blood 2011;115:2731–9.
5. Kralovics R, Passamonti F, Buser AS, Teo SS, Tiedt R, Passweg JR, et al. A gain-of-function mutation of JAK2 in myeloproliferative disorders. N Engl J Med 2005;352:1779–90.
6. Chapman JR, Taylor MR, Boulton SJ. Playing the end game: DNA double-strand break repair pathway choice. Mol Cell 2012;47:497–510
7. Gaymes TJ, Mufti GJ, Rassool FV. The non homologous end-joining pathway is aberrant in human myeloid leukemias: Evidence that KU70/86 is required for the increased frequency of misrepair. Cancer Res 2002;62:2791–7.
8. Brady N, Gaymes TJ, Cheung M, Mufti GJ, Rassool FV. Increased error-prone NHEJ activity in myeloid leukemias is associated with DNA damage at sites that recruit key nonhomologous end-joining proteins. Cancer Res 2003;63:1798–805.
9. Rassool FV, Gaymes TJ, Omidvar N, Brady N, Beurlet S. Pla reactive oxygen species, DNA damage, and error-prone repair: A model for genomic instability with progression in myeloid leukemia? Cancer Res 2007;67:8762–71.
10. Sallmyr A, Fan J, Datta K, Kim KT, Grosu D, Shapiro P, et al. Internal tandem duplication of FLT3 (FLT3/ITD) induces increased ROS production, DNA damage, and misrepair: Implications for poor prognosis in AML. Blood 2008;111:3173–82.
11. Heiss E, Masson K, Sundberg C, Pedersen M, Sun J, Bengtsson S, Rönnstrand L. Identification of Y589 and Y599 in the juxtamembrane domain of Flt3 as ligand-induced autophosphorylation sites involved in binding of Src family kinases and the protein tyrosine phosphatase SHP2. Blood 2006;108:1542–50
12. Razumovskaya E, Sun J, Rönnstrand L. Inhibition of MEK5 by BIX02188 induces apoptosis in cells expressing the oncogenic mutant FLT3-ITD. Biochem Biophys Res Commun 2011;412:307–12.
13. Pradhan A, Lambert QT, Reuther GW. Transformation of hematopoietic cells and activation of JAK2-V617F by IL-27R, a component of a heterodimeric type I cytokine receptor. Proc Natl Acad Sci U S A 2007;104:18502–7
14. Pierce AJ, Johnson RD, Thompson LH, Jasin M. XRCC3 promotes homology-directed repair of DNA damage in mammalian cells. Genes Dev 1999;13:2633–8.
15. Richardson C, Moynahan ME, Jasin M. Double-strand break repair by interchromosomal recombination: Suppression of chromosomal translocations. Genes Dev 1998;12:3831–42.

16. Luria SE, Delbrück M. Mutations of bacteria from virus sensitivity to virus resistance. Genetics 1943;28:491–511.
17. Seedhouse CH, Hunter HM, Lloyd-Lewis B, Massip AM, Pallis M, Carter GI, et al. DNA repair contributes to the drug-resistant phenotype of primary acute myeloid leukaemia cells with FLT3 internal tandem duplications and is reversed by the FLT3 inhibitor PKC412. Leukemia 2006;20:2130–6
18. Raderschall E, Stout K, Freier S, Suckow V, Schweiger S, Haaf T. Elevated levels of RAD51 recombination protein in tumor cells. Cancer Res 2002;62:219–25
19. Marty C, Lacout C, Droin N, Le Couédic JP, Ribrag V, Solary E, et al. A role for reactive oxygen species in JAK2 V617F myeloproliferative neoplasm progression. Leukemia 2013;27:2187–95
20. Skopek TR, Liber HL, Penman BW, Thilly WG. Isolation of a human lymphoblastoid line heterozygous at the thymidine kinase locus: Possibility for a rapid human cell mutation assay. Biochem Biophys Res Commun 1978;84:411–6.
21. Zeigler FC, Bennett BD, Jordan CT, Spencer SD, Baumhueter S, Carroll KJ, et al. Cellular and molecular characterization of the role of the flk-2/flt-3 receptor tyrosine kinase in hematopoietic stem cells. Blood 1994;84: 2422–30.
22. Lee BH, Tothova Z, Levine RL, Anderson K, Buza-Vidas N, Cullen DE, et al. FLT3 mutations confer enhanced proliferation and survival properties to multipotent progenitors in a murine model of chronic myelomonocytic leukemia. Cancer Cell 2007;12:367–80.
23. Shide K, Shimoda HK, Kumano T, Karube K, Kameda T, Takenaka K, et al. Development of ET, primary myelofibrosis and PV in mice expressing JAK2 V617F. Leukemia 2008;22:87–95
24. Mohamedali A, Gäken J, Twine NA, Ingram W, Westwood N, Lea NC, et al. Prevalence and prognostic significance of allelic imbalance by single-nucleotide polymorphism analysis in low-risk myelodysplastic syndromes. Blood 2007;110:3365–73.
25. Gaymes TJ, Mohamedali AM, Patterson M, Matto N, Smith A, Kulasekararaj A, et al. Microsatellite instability induced mutations in DNA repair genes CtIP and MRE11 confer hypersensitivity to poly (ADP-ribose) polymerase inhibitors in myeloid malignancies. Haematologica 2013;98:1397–406.
26. Melcher R, Al-Taie O, Kudlich T, Hartmann E, Maisch S, Steinlein C, et al. SNP-Array genotyping and spectral karyotyping reveal uniparental disomy as early mutational event in MSS- and MSI-colorectal cancer cell lines. Cytogenet Genome Res 2007;118:214–21.
27. Perrotti D, Jamieson C, Goldman J, Skorski T. Chronic myeloid leukemia: Mechanisms of blastic transformation. J Clin Invest 2010;120:2254–64.
28. Zhang X, Tang N, Hadden TJ, Rishi AK. Akt, FoxO and regulation of apoptosis. Biochim Biophys Acta 2011;1813:1978–86.
29. Klein HL.The consequences of Rad51 overexpression for normal and tumor cells. DNA Repair 2008;7:686–93.
30. Trachootham D, Zhang H, Zhang W, Feng L, Du M, Zhou Y, et al. Effective elimination of fludarabine-resistant CLL cells by PEITC through a redox-mediated mechanism. Blood 2008;112:1912–22.